# The interaction between active aeroelastic control and structural tailoring in aeroservoelastic wing design

Binder, Simon; Wildschek, Andreas; De Breuker, Roeland

**DOI**
10.1016/j.ast.2021.106516

**Publication date**
2021

**Document Version**
Final published version

**Published in**
Aerospace Science and Technology

Aerospace Science and Technology 110 (2021) 106516

Contents lists available at ScienceDirect

Aerospace Science and Technology

www.elsevier.com/locate/aescte

# The interaction between active aeroelastic control and structural tailoring in aeroservoelastic wing design

Simon Binder [a,b,*], Andreas Wildschek [c], Roeland De Breuker [b]

[a] Materials X, Airbus Defence and Space GmbH, Germany
[b] Section of Aerospace Structures and Computational Mechanics, Faculty of Aerospace Engineering, Delft University of Technology, the Netherlands
[c] Aircraft Control Domain, Airbus Operations SAS, France

ARTICLE INFO

*Article history:*
Received 5 February 2020
Received in revised form 19 August 2020
Accepted 13 January 2021
Available online 18 January 2021
Communicated by Grigorios Dimitriadis

*Keywords:*
Aeroservoelastic optimization
Composite tailoring
Feed-forward gust load control
Manoeuver load alleviation

ABSTRACT

This paper presents an analysis of the interaction and trade-off between active aeroelastic control and passive structural tailoring on a free-flying fully flexible aircraft model. Both technologies are included in the preliminary design of a typical transport aircraft configuration with a conventional control surface layout containing trailing edge control surfaces and spoilers. The passive structural tailoring is facilitated by exploiting the anisotropic properties of composite materials to steer the static and dynamic aeroelastic behaviour. Active aeroelastic control is implemented by scheduled control surface deflections redistributing the aerodynamic loads during manoeuvres to achieve manoeuvre load alleviation and a feed-forward control law for gust load alleviation. The panel-based aerodynamic modelling of spoiler deflections is improved by a correction of the spatial distribution of the boundary condition derived from higher fidelity simulation data. The optimisation of active control laws requires the consideration of constraints of the actuation system, namely rate and deflection saturation, in a nonlinear manner. The interaction of manoeuvre load alleviation, gust load alleviation and passive structural tailoring is investigated on the basis of results of different aeroservoelastic optimisations. Therefore the primary wing structure is simultaneously optimised with the individual technologies being activated or deactivated, resulting in eight different wing structures. The results of the individual and combined optimisations reveal significant design differences. The potentials of the different technologies can only be optimally exploited by simultaneous optimisation. The paper concludes with a study of the sensitivity of the major findings with respect to the knockdown factor for failure applied to the material properties. A substantial shift of effectiveness from active aeroelastic control to passive structural tailoring is observed with increased allowables resulting in more flexible and hence less stiff wing designs.


## 1. Introduction

The introduction of composite materials was an important milestone in the development of lightweight wing structures. However, costly manufacturing, high repair costs and complex recycling processes put the advantages of the high strength to weight ratio into perspective. In fact, full exploitation of the material properties is required for composite materials to compete with well established metallic structures [1]. An important step in fully exploiting the anisotropic material properties of carbon fibre reinforced plastics has been the industrial utilisation of automated processes for producing tow-steered composites. While the method allows improving the aeroelastic behaviour by introducing beneficial aeroelastic couplings passively, the interaction with active control systems is affected. The analysis thereof is the subject of this work.

In aviation, the exploitation of anisotropic material properties has its origin 70 years ago in the development of wooden propellers in which the fibre direction was utilised to create the desired aeroelastic behaviour [2]. This method, also known as structural tailoring, is defined as the steering of the aeroelastic behaviour by structural design so that it is favourable for the particular performance target. In terms of wing development, structural tailoring by the embodiment of directional stiffness promises various enhancements of the aircraft performance. The early studies have concentrated on the beneficial effects of the induced stiffness cross-coupling on static and dynamic aeroelastic stability, control surface effectiveness and load redistribution for manoeuvre load alleviation and lift efficiency [3]. Further studies also revealed the positive influence of structural tailoring on the dynamic characteristics relevant for gust encounters [4], [5]. Motivated by the

* Corresponding author at: Kluyverweg 1, 2629 HS Delft, the Netherlands.
*E-mail address:* s.binder-1@tudelft.nl (S. Binder).

https://doi.org/10.1016/j.ast.2021.106516

promising results, directional stiffness was included as a parameter in the field of multidisciplinary aircraft wing optimisations. While most optimisation studies aim to reduce the mass of the primary structure [6] [7], others seek to further increase the fuel efficiency of aircraft by additionally improving the lift-to-drag ratio in static trim conditions [8]. In recent years, the investigation of the influence of directional stiffness on the dynamic behaviour of box-like wing structures has received more attention [9], [10].

Stodieck et al. [11] recently investigated the application of tow-steering in the design of composite wing boxes. With the inclusion of control surface effectiveness constraints, it became apparent that depending on the design driving constraints, different mechanisms occur. While load alleviation for manoeuvre and gusts requires wash-out, control surface effectiveness and flutter speed were raised by inducing a wash-in behaviour by structural tailoring.

Contrary to passive methods for influencing the aeroelastic behaviour, active means have been investigated since decades. An important distinction from passive methods results from the ability of the active control methods to adapt to the particular flight conditions such as fuel state, payload configuration or centre of gravity position. The active control systems considered in this work are Manoeuvre Load Alleviation (MLA) and Gust Load Alleviation (GLA).

Both technologies have been applied to various aircraft [12] and target the alleviation of aerodynamic loads by control surface deflections in a way that is beneficial for the structural design. Concerning MLA, the redistribution of aerodynamic loads by control surface deflections mostly involves a shift of the centre of pressure inboard and thus closer to the wing root resulting in a reduced bending moment. Gust Load Alleviation targets the reduction of the loads encountered during turbulent flight conditions by dynamic control surface deflections. Feeding back the signal of sensors as accelerometers to control surface actuators can artificially increase the damping of specific aeroelastic modes and thereby lower the structural loads. Instead of modifying the response, these control surface deflection commands can also be computed by feeding forward a filtered signal of a turbulence measurement taken upfront the aircraft. Both ways, the control surface deflections lead to redistributed aerodynamic loads when encountering turbulence.

Besides the influence that GLA has on the dynamic response of an aircraft, the similarity in the mechanisms of structural tailoring and MLA, as well as the conflicting requirements on the bending-torsion coupling, suggests that strong interaction is expected when using both technologies on a single wing. Weisshaar predicted that the designers of active control systems for composite wings would have not only to examine the effect of changing the gains but also the effects of structural tailoring on the resulting control law [13]. The interaction and the associated issues or synergies have led to a variety of studies and projects to address the so-called field of aeroservoelasticity. The general aspects of aeroservoelastic modelling, analysis and optimisation, as well as relevant applications, are summarised in [14].

Dealing with aircraft wings on a simplified and general level, the studies of Zeiler and Weisshaar [15], Librescu et al. [16] and Weisshaar and Duke [17] have been, amongst others, pointing the way. In the study performed by Zeiler et al. [15], the synergistic potential of integrated structural and control design was revealed in a wing optimisation with the objective of aeroelastic stability increase. More specifically, specific changes in the structural design showed an increase in the controllability of modes that were otherwise nearly uncontrollable [15]. This beneficial effect was also observed by Librescu et al. [16] when extending the concept to anisotropic, composite wing structures. It was shown that the combined optimisation outperforms either structural tailoring or active control alone [16]. Weisshaar and Duke [18] investigated the combined use of active control and structural tailoring with the objective of drag reduction. With combined use, the induced drag can be minimised with smaller control surface deflections, but the determination of the deflections requires a combined optimisation with the structure.

Over the years and as the tools and methods for integrated aeroservoelastic analysis and optimisation have evolved, many applications have been presented that target the integrated preliminary design of transport aircraft wings.

Integrating active manoeuvre and gust load control in the preliminary aircraft design was shown to have a drastic impact on the resulting optimal overall design [19]. Many studies exist in which transport aircraft wing structures with isotropic material properties are optimised concurrently with flutter control, GLA, MLA and shape adaption by morphing [20], [21], [22], [23], [24].

The interaction of structural tailoring and active control was studied by Handojo et al. [25] using the example of optimisation of a composite wing in the presence and absence of a fixed control law for manoeuvre and gust load alleviation. However, in the applied sequential optimisation, the optimiser couldn't fully utilize the directional stiffness properties as the sensitivity of the loads with respect to the structural design parameters was invisible to the optimiser. As a result, the optimiser was unable to exploit the potential of the directional stiffness properties to redistribute and alleviate the loads.

Integrated design of subsonic transport aircraft composite wings employing structural tailoring and active trailing edge morphing for manoeuvre load alleviation has been presented by Werter [26] finding that design difference occur both in the stiffness distribution as well as the morphing induced camber distribution whether or not the other technology is accounted for. A similar investigation was carried out by Krupa et al. [27], who simultaneously optimised a wing structure including the control surface deflections for active manoeuvre load alleviation. As expected, the wing employing both technologies outperformed the designs employing one of the two.

The previously given examples were focused either on single technologies or combinations of structural tailoring with manoeuvre load alleviation or flutter control. The interaction between active gust load alleviation and structural tailoring in the integrated optimisation of composite wings has not been studied on the example of transport aircraft configurations. The above-listed examples that include active control and structural tailoring consider either single control surfaces or distributed control surfaces located at the trailing edge. The following points differentiate the present work from the mentioned studies:

- Instead of individual considerations or pairwise combinations, an analysis of the interaction between the three technologies of structural tailoring, manoeuvre load alleviation, and gust load alleviation is presented as the tailored utilization of directional stiffness properties affects both, manoeuvre and gust loads.
- Instead of single control surfaces or idealised layouts, a typical transport aircraft configuration is used with a conventional control surface layout consisting of spoilers and ailerons that is compatible to the current state of the art.
- The influence of the structural flexibility on the observed interactions and the trade-off between active and passive load alleviation is analysed by a continuous variation of the material properties. This enables the assessment of the extent to which the results retain validity in case of variations.

Various optimisations of the wing structure are carried out with the individual technologies and their combinations to understand

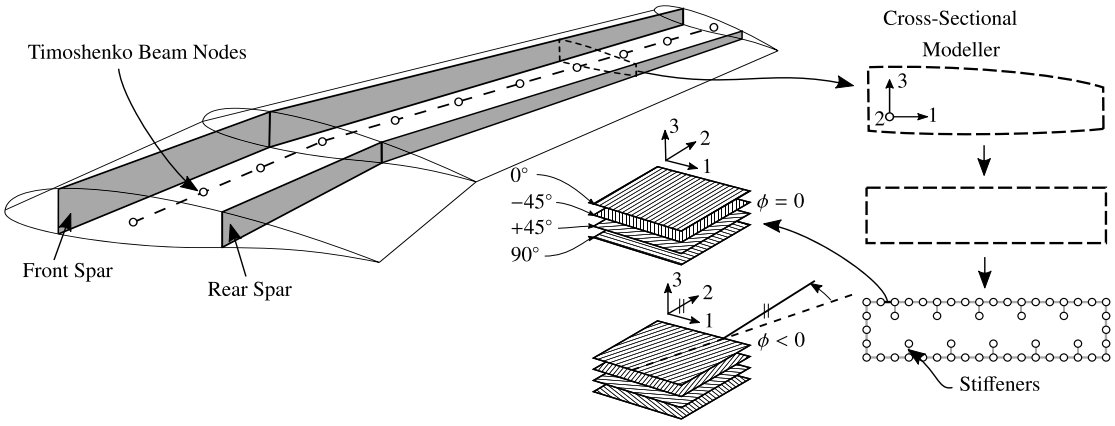


**Fig. 1.** Structural modelling approach using Timoshenko beam elements with stiffness and mass properties obtained by the cross-sectional modeller. Explanation of the reference angle or principal stiffness direction $\phi$.

the mechanisms behind the three technologies. Optimisations are carried out including static and dynamic aeroelastic constraints including strength and buckling constraints resulting from manoeuvre and gust flight conditions. For the consideration of structural tailoring, a predefined laminate lay-up is used that complies with the usual composite design guidelines used in the industry. The actual parameter for including stiffness direction in the optimisation is the reference direction of the plies. The MLA is included by scheduled control surface deflections during the steady symmetric load conditions, i.e. pull-up or push-over manoeuvre, and antisymmetric load conditions, i.e. rolling manoeuvres. A stack of finite impulse response filters is optimised alongside the other design parameters to emulate the presence of an optimal feed-forward gust load alleviation system. The paper concludes by answering the remaining question whether the observed interactions are robust to variations in the selected material by a sensitivity analysis of the major findings with respect to the knockdown factor applied to the material properties.

## 2. Aeroservoelastic model

The integrated aeroservoelastic design studies carried out in this work are performed with the open-source toolchain dAEDalus that has been originally developed to investigate the effects of aeroelasticity on the handling qualities during preliminary aircraft design [28]. Among other developments, the capability of numerical optimisation was included in the course of this work. The following introduces the models of structural dynamics, aerodynamics and active control required for the aeroservoelastic optimisation.

### 2.1. Structural model

The equations of motion of the structural dynamics are based on the finite element method. Linear Timoshenko beam elements are used for the discretisation of the aircraft structure on a global level. The stiffness and mass properties of the thin-walled wing cross-sections are obtained by the cross-sectional modeller developed by Ferede and Abdalla [29]. The implementation used in the course of this work has been adopted from Proteus, a toolchain developed by Werter and De Breuker [30] for the structural optimisation of aeroelastically tailored wing structures.

On the cross-sectional level, the geometry of the cross-section is first discretised with two-dimensional shell elements, as shown in Fig. 1. The outer dimensions of the cross-sections result from predefined spar positions and airfoils. The height of the front and rear spar is assumed to be equal. On the laminate level, the layup is specified by the stacking sequence of the individual ply directions.

With the stiffness and mass information obtained on the cross-sectional level, the Timoshenko beam element stiffness and mass matrices are obtained. The global stiffness and mass matrix are thereafter assembled. The full stiffness and mass matrix are used for the static structural analyses, whereas a representation based on modal coordinates is employed in the dynamic structural model. A mean-axis approach is utilised for the realisation of the equations of motion of the free-flying flexible body, as used by Seywald [28].

### 2.2. Aerodynamic model

The steady aerodynamic model in dAEDalus is based on the well-known Vortex Lattice Method (VLM) [31]. The unsteady aerodynamic model is based on a continuous-time state-space formulation of the Unsteady Vortex Lattice Method (UVLM) that has been first described by Mohammadi et al. [32] for two-dimensional airfoils, formulated for three-dimensional lifting surfaces by Werter et al. [33], and extended for arbitrary motion and control surface deflections by the authors [34]. The aerodynamic solvers in dAEDalus are based on the well-known Vortex Lattice Method (VLM) [31] for steady aerodynamics and the Unsteady Vortex Lattice Method (UVLM) [32] for unsteady aerodynamics. The latter has been formulated for three-dimensional lifting surfaces by Werter et al. [33], and extended for arbitrary motion and control surface deflections by the authors [34]. In both methods, control surfaces are realised by a modification of the boundary conditions imposed on the respective control surface panels. The modification is equivalent to a rotation of the panels associated with the control surface around the hinge axis. The control surface deflection thereby leads to a different flow field in which mainly the circulation near the control surface is changed.

The control surface layout used in this work also includes spoilers for which this type of modelling, i.e. the mere modification of the boundary condition imposed on the spoiler panels, produces unsatisfactory results. The flow around a deployed spoiler, i.e. exhibiting large deflections, is highly dominated by effects that are not accounted for by potential flow methods, e.g. regions of separated flow behind the spoiler. In the following, the derivation of a correction method is shown to improve the accuracy of modelling spoilers with the vortex lattice method. The boundary condition is therefore modified for all panels in the spanwise region of the spoiler instead of only the spoiler panels.

The linearity of the vortex lattice model allows an inverse computation of the required incremental boundary condition $\mathbf{b}_{\text{req}}$ that

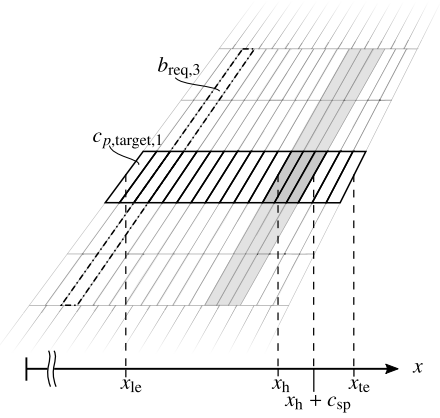


**Fig. 2.** Aerodynamic panel mesh in the area of a spoiler control surface. The panels chosen for the derivation for a correction law are highlighted in bold. The dash-dotted line indicates the area in which the boundary condition is varied simultaneously.

results in a given incremental pressure distribution $\mathbf{c}_{p,\text{target}}$ by solving the linear system of equations:

$$\left(\frac{\partial c_{p,i}}{\partial b_j}\right)_{(i=1..n_p, j=1..n_p)} \mathbf{b}_{\text{req}} = \mathbf{c}_{p,\text{target}} \tag{1}$$

with $\partial c_{p,\text{i}}/\partial b_j$ being the influence that an increment in the boundary condition of the $j$-th panel has on the pressure coefficient of the $i$-th panel. These differentials are obtained by a transformation of the influence coefficients that are naturally available using the VLM.

To provide a correction that is usable for different shapes and positions of spoilers, the set of panels considered in the target pressure distribution is limited to a set of panels in the area of the midspan of the spoiler surface, which are the bold panels in Fig. 2. Furthermore, the boundary condition is varied simultaneously for all spanwise panels of a row in chordwise direction in the region of the spoiler. As an example, the combination of the panels of the third row, resulting in the combined boundary condition $b_{\text{req},3}$, is indicated by the dash-dotted line in Fig. 2.

The target pressure distribution used here is calculated from data obtained by a commercial CFD solver based on Reynolds Averaged Navier Stokes (RANS) equations. The CFD computations were carried out on the wing of the NASA Common Research Model (CRM [35]) for one flight condition with and without spoiler deflection and subsequently mapped to an equivalent panel mesh.

The chordwise distributed boundary condition that matches a sectional pressure distribution obtained by the CFD calculation is shown in Fig. 3 and is indicated by the adjective optimal. The boundary condition is normalised to the equivalent boundary condition obtained by a conventional rotation of the panels resulting in the boundary condition factors $b/b_{\text{rot}}$. The chordwise distribution of a conventional rotation of the panels associated to the spoiler surface is shown for comparison.

A simplified distribution is obtained by an approximation of the optimal distribution by piecewise linear segments between the four chordwise stations indicated in Fig. 3 by the vertical lines:

$$\begin{aligned} b(x_{\text{le}}) &= -0.075 b_{\text{rot}} \\ b(x_{\text{h}} - c_{\text{sp}}) &= -0.2 b_{\text{rot}} \\ b(x_{\text{h}} + 0.5 c_{\text{sp}}) &= 1.1 b_{\text{rot}} \\ b(x_{\text{te}}) &= 0.5 b_{\text{rot}} \end{aligned} \tag{2}$$

Herein, $x_{\text{le}}$, $x_{\text{te}}$ and $x_{\text{h}}$ denote the chordwise position of the leading edge, trailing edge and spoiler hinge axis, and $c_{\text{sp}}$ denotes the chord of the spoiler control surface.

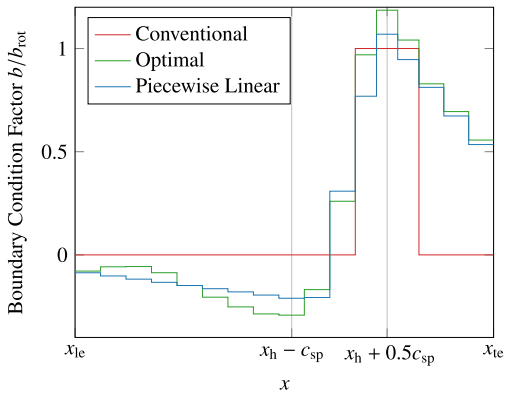


**Fig. 3.** Comparison of the boundary condition required to match the pressure distribution obtained by CFD simulation with the conventional boundary condition. The piecewise linear approximation represents the simplified correction that is usable for different shapes and positions of spoiler control surfaces.

The resulting integrated sectional lift and moment coefficients for various spoiler deflections are shown in Fig. 4. The correction improves the otherwise poor performance of the VLM, especially in calculating the moment coefficient. In the present case, CFD data were used for the correction at a moderate spoiler deflection of 15 degrees, which is expected to be sufficient for load alleviation functions. Due to the linear nature of the VLM cannot account for the nonlinear effects such as local flow separation that are observed in the CFD results for higher deflections. The derived correction law is implemented for all spoiler control surfaces in the aerodynamic models used in this work. However, due to the lack of appropriate simulation data, it was not investigated, to which extend the correction method found is applicable for unsteady aerodynamic models.

Before the integration with the structural and flight dynamic equations of motion, the computational complexity of the unsteady aerodynamic state space model is reduced by model order reduction (MOR). The reduced order model is established by a method that combines the balanced proper orthogonal decomposition with the concept of synthetic mode shapes [36]. The method is especially suitable for the reduction of models used in aeroservoelastic optimisation as it requires no prior knowledge of the structural dynamics.

Coupling the aerodynamic model to the equations of motion of the free-flying flexible body requires the transformation of aerodynamic loads to structural loads and the transformation of structural motion to the motion of the panels. The generation of the required coupling matrices, as well as the integration of the models used in this work, is described by the authors in detail in Ref. [37].

### 2.3. Active aeroelastic control

The presence of an MLA control law is simulated by commanding control surface deflections $\delta_{\text{MLA}}$ during the static analysis of the manoeuvre conditions. For push-over and pull-up manoeuvres, these control surface deflections are symmetric, i.e. the deflections on the right wing equal the deflections of the control surfaces on the left wing. In case of asymmetric load conditions, e.g. a roll manoeuvre, the symmetric deflections are additionally superimposed by a vector of antisymmetric control surface deflections $\delta_{\text{MLA,asym}}$.

The GLA control law is modelled by the secondary feed-forward path that is shown in Fig. 5. The vertical flow velocity $w$ is sensed by an Angle Of Attack (AOA) sensor located at the nose of the aircraft. The measured variation in angle of attack $\alpha_{\text{meas}}$ is high pass filtered to prevent the feed-forward controllers from trying to alleviate the trim angle of attack. The resulting signal $\bar{\alpha}_{\text{meas}}$ is then

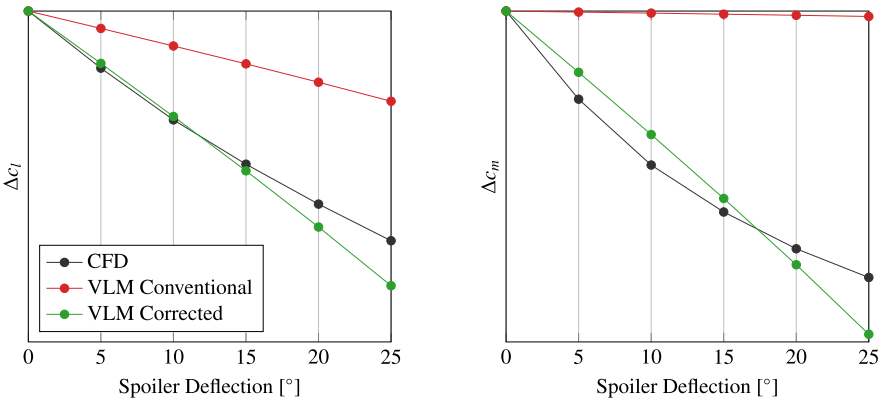


**Fig. 4.** Spoiler induced increment in sectional lift $\Delta c_l$ and sectional moment $\Delta c_m$ for various spoiler deflections obtained by CFD, the conventional VLM without correction and the corrected VLM.

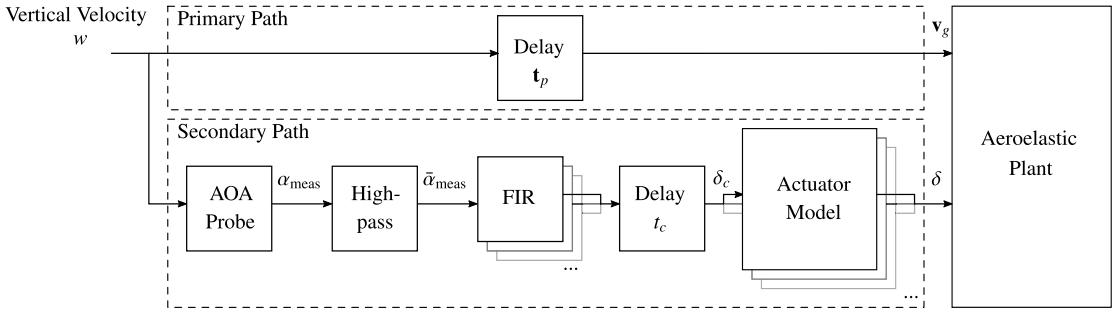


**Fig. 5.** Control scheme used to emulate the presence of an optimal gust load control law during the structural optimisation.

passed to the stack of Finite Impulse Response (FIR) filters associated to the individual control surface pair. Thereby, one FIR filter is used per control surface pair consisting of left and right control surface. The $z$-transfer function of an FIR filter of order $N$ can be written as [38]:

$$H_{\mathrm{FIR}}(z) = \sum_{n=1}^{N} h_n z^{-n+1} \tag{3}$$

with $h_n$ being the $n$th element of the vector of FIR filter coefficients $\mathbf{h}$.

The subsequent delay $t_c$ accounts for the time required by the fictitious controller for the computation of the control surface deflection commands $\delta_c$. The actuators for each control surface pair are modelled as nonlinear second-order systems with rate and deflection limits. After the commanded signals $\delta_c$ have been processed by the actuator models of the individual control surfaces, the resulting actual deflections $\delta$ are forwarded to the aeroelastic model.

In parallel, the vertical flow velocity $w$ is delayed before it is passed to the gust zone inputs $\mathbf{v}_g$ of the aeroelastic model, see the lower path in Fig. 5. The different delays in the vector of time-delays $\mathbf{t}_p$ depend on the flight speed and the distance between the reference point, i.e. the aoa probe, and the aerodynamic centres of the individual gust zones.

It should be noted that in this work, the assumption of one-dimensional turbulence profiles results in an exact measurement of the gust velocity at only one spanwise station. Furthermore, no uncerntainty in the delay $t_c$ and properties of the actuator transfer function are taken into account. Under these circumstances, the feed-forward path used here can be considered as a highly idealised gust load controller.

## 3. Aeroservoelastic analysis and optimisation

For the optimisations required in this work, static and dynamic aeroservoelastic analyses are performed after integrating the models of aerodynamics, structure and control described in the previous section. This section describes the principal methodology of steady manoeuvre and dynamic gust analysis as well as the general aspects of the optimisation problem formulation.

### 3.1. Analysis

The analysis of quasi-steady manoeuvre conditions is done by finding the static equilibrium between inertial and aerodynamic forces acting on the aircraft. The iterative search of the required angle of attack, angle of sideslip and control surface deflections eliminates the need for the trim parameters to be design variables in the optimisation problem. For symmetric cases, the angle of attack and the elevator deflection are used as trim parameters to find the longitudinal equilibrium between weight forces and the required lift. The asymmetric roll manoeuvre condition also requires the equilibrium of lateral forces. Therefore, the trimming parameters additionally include antisymmetric control surface deflections $\delta_{\mathrm{MLA,asym}}$ and the sideslip angle $\beta$. As multiple control surfaces can be used for roll control, the weights of the individual deflection are used as design variables defining the roll allocation $\bar{\delta}_{\mathrm{MLA,asym}}$. A single amplification parameter $r$ is then used within the trimming routine that is multiplied with the vector of weights to find the actual individual control surface deflections:

$$\delta_{\mathrm{MLA,asym}} = r\bar{\delta}_{\mathrm{MLA,asym}} \tag{4}$$

For the dynamic analysis of gust encounters during horizontal flight conditions, the simulation of the free-flying flexible body is performed in the time domain in three steps:

1. The discrete transfer functions of the FIR filters, compare Eq. (3), are transformed in the time domain by a bilinear transformation, and the control surface commands $\delta_c$ due to the gust profiles are computed as depicted in Fig. 5.
2. The continuous-time signal of commanded control surface deflections is subsequently used in the nonlinear simulation of the actuator, including actuator rate limitations and deflection saturation.
3. The resulting actual control surface deflection histories $\delta$ are used alongside with the gust profiles in a linear time-domain simulation of the overall aircraft dynamics.

Subsequently, structural failure is assessed by the computation of strength and buckling reserve factors with the wing deformation resulting at the obtained equilibrium points of the steady cases and the time history of the dynamic analysis. Similar to the approach used by Werter [26], the strength failure criterion is based on the work of IJsselmuiden et al. [39], and the buckling reserve factors are computed by a buckling analysis based on the work of Dillinger et al. [40]. It should be noted that only local buckling is taken into account with the buckling panels being bounded by ribs and stiffeners. For computational reasons, the buckling reserve factors during gust encounters are computed only for the maximum principal strains obtained in the dynamic analysis.

### 3.2. Optimization problem formulation

The objective of all design optimisations carried out in the current work is the reduction of the mass of the primary wing-box structure, i.e. the skin and spars.

The design parameters include structural and control design variables. Four variables are used for the thickness of skins and spars in each beam element, i.e. no chordwise variation of the thickness is allowed and the stringer thickness is held constant. The local minimum allowable value for the material thickness is defined based on requirements resulting from manufacturing, handling and uncontained engine failure cases. While the layup is held constant throughout the optimisation process, only the ply thickness is varied to ensure a continuous design space. Besides the laminate thickness variables, the laminate principal stiffness direction is optimised in the form of a distribution of the reference angle $\phi$ for the 0° ply direction as shown in Fig. 1. The spanwise distribution of the principal stiffness direction is therefore formulated as a linear combination of Chebyshev polynomials:

$$\phi(\eta) = \sum_{i=1}^{n} c_{\phi,i} \frac{\left(\eta + \sqrt{\eta^2 - 1}\right)^{n-1} + \left(\eta - \sqrt{\eta^2 - 1}\right)^{n-1}}{2} \tag{5}$$

where $n$ denotes the number of polynomials used. The vector of coefficients $\mathbf{c}_\phi = [c_{\phi,1}, c_{\phi,2}, ...., c_{\phi,n}]^T$ is used as the structural tailoring design variable. A similar approach based on B-splines has been used by Stodieck et al. [11] to ensure smooth property variations along the span.

The MLA design space is spanned by a vector of commanded control surface deflections $\delta_{\text{MLA}}$ for each load case and additionally the roll allocation weights $\delta_{\text{MLA,asym}}$ for asymmetric conditions as roll manoeuvres. Finally, the GLA design variables consist of one vector of FIR filter coefficients $\mathbf{h}$ for each control surface pair that is used for dynamic gust load control.

Various constraints $c \in \mathcal{R} > 0$ are used to form the feasible region that is defined as $c \leq 1$ in the design space. For each component of the wingbox structure, i.e. front spar, rear spar, upper skin, and lower skin, one buckling and one strength constraint are formulated for each beam element and flight condition. The constraints resulting from the time histories of all gust analyses, i.e. with the various gust gradients considered, are aggregated to one constraint using the Kreisselmeier-Steinhauser functions [41]. By this, the gust analysis results in one buckling and one strength constraint per beam element and wingbox component.

The maximum and minimum control surface deflections used for MLA are bounded for symmetric flight conditions and formulated as constrains for roll conditions. The control surface rate and deflections occurring during gust encounters are limited by the actuator models resulting in an always feasible GLA feed-forward path. A damping constraint is used a gust analysis speed, ensuring a stable dynamic system for numerical purposes during the time domain gust analyses.

It should be noted that flutter margins and flutter control are not considered in the course of this work. However, for numerical reasons, the dynamic stability is constrained at the speeds at which the gust analyses are carried out.

A single optimisation problem is formulated that consists of structural and control design variables to minimise the wingbox structural mass with respect to the constraints described above. An active set algorithm is used to reduce the complexity of the search for the optimal solution by considering only a subset of constraints which are active at the current design point. The gradient-based optimisation algorithm requires the computation of a Jacobian matrix at every optimisation iteration. The sparsity of this Jacobian is exploited by an efficient procedure that runs only the required analyses, e.g. as the GLA design variables do not affect manoeuvre constraints, the respective gradients are zero and do not need to be computed by finite differentiation.

## 4. Analysis and results

The previously described models and analysis procedures are now used for the optimisation of an aircraft wing structure. After a description of the test case, eight optimisations are carried out with the individual technologies, i.e. MLA, GLA and structural tailoring, being activated or deactivated. Based on the resulting designs, the interaction of manoeuvre load alleviation, gust load alleviation and passive structural tailoring is investigated next. A study of the sensitivity of the major findings with respect to the knockdown factor applied to the material properties is presented at the end of the section.

### 4.1. Test case description

The analyses and optimisations presented in this work are conducted on a generic long-haul transport aircraft model. The configuration belongs to category 4E (ICAO/EASA aerodrome reference code) and has a Maximum Take-Off Weight (MTOW) of more than 250,000 kg.

The airframe structure is made from AS4/3501-6 composite material. The individual layers of unidirectional tape are placed in an angle of 0°, 90° and ±45° relative to the reference direction. The layup is also defined by fixed percentages of the individual layer directions. Furthermore, only symmetric and balanced layups are considered. Tailoring is exerted in the wing skins only, the primary stiffness direction of the spars coincides with the beam axis. This means that the desired bending torsion coupling is only achieved by modifying the extension shear coupling in the skins. The maximum number of the Chebyshev polynomials used as shape functions for the distribution of the reference angle $\phi$ is set to five. The wing structure is discretised using 34 beam elements.

The employed conventional control surface layout consists of six spoiler control surfaces as well as an inner and an outer aileron as shown in Fig. 6. All wing control surfaces are used for manoeuvre load alleviation and roll control while for gust load alleviation, only the outer three spoilers and the ailerons are used. While the

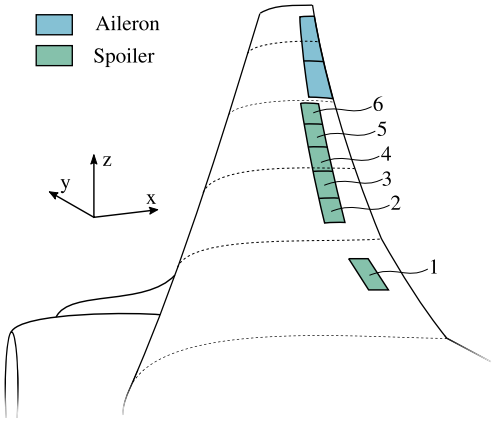


**Fig. 6.** Schematic drawing of the used conventional control surface layout consisting of six spoilers and the inner as well as the outer aileron.

**Table 1**
Summary of the Design Space.

| Design Variables | |
|---|---|
| Laminate Thickness (Skins and Spars; $\mathbf{t}$) | $4 \cdot 17$ |
| Tailoring (Upper and Lower Skin; $\mathbf{c}_\phi$) | $2 \cdot 5$ |
| MLA ($\delta_{\text{MLA}} + \bar{\delta}_{\text{MLA,asym}}$) | $4 \cdot 8$ |
| GLA ($\mathbf{h}$) | $16 \cdot 5$ |
| Total | 190 |

actuation characteristics, i.e. maximum rate, natural frequency and damping are the same for the spoilers and the ailerons, the downward deflection limits differ. Aileron deflections are symmetric to the zero position whereas spoilers can only be deflected upwards. An order of 16 is used for the FIR filter of each control surface used for gust load alleviation.

The aerodynamic model includes wing and tail lifting surfaces, and no aerodynamic fuselage is considered. The panel mesh consists of more than $10^4$ panels. The configuration is divided into 10 gust zones to account for the delay occurring when the gust moves along the aircraft.

The constraints are evaluated at three, previously selected representative manoeuvre flight conditions: a $2.5g$ pull-up manoeuvre, a $-1g$ push-over manoeuvre and a roll manoeuvre with a predefined roll rate at a load factor of $1.67g$. The gust analysis is carried out at the design speed in the MTOW configuration. The analysis includes 15 discrete gust gradients analysed in a range from nine to 107 m as specified by the certification specifications for large aeroplanes [42]. Updraught and downdraught gust conditions are considered. The modal basis used for the dynamic analysis consists of 31 modes, including the six rigid-body modes.

For the given test case, the design space results in 190 design variables that are summarised in Table 1. The starting point of all optimisations is an over-sized but feasible structure. The design variables associated with MLA, GLA or structural tailoring are initialised with a zero value. Only the wing structure is optimised while the remaining airframe is fixed throughout the optimisation.

The optimisations are stopped when the change in the wingbox mass between two iterations is less than 0.01 kg, and the constraints are satisfied within a tolerance of $10^{-4}$.

### 4.2. Individual and combined methods for mass reduction

Various optimisations are carried out in which the different methods are active or inactive to investigate the influence of the different technologies on the primary wing structural mass. Table 2 shows the various performed optimisations together with the active and inactive subsets of the design variables. The reference

**Table 2**
Description of the various optimisation configurations with active (✓) and inactive (-) subsets of design variables and the resulting mass reduction normalised to the maximum achievable mass reduction obtained by the concurrent optimisation with all design variables (TMG).

| Setup | Design Variable Subsets | | | | Normalised Weight Reduction |
|---|---|---|---|---|---|
| | Thickness | Tailoring | MLA | GLA | |
| N | ✓ | - | - | - | - |
| T | ✓ | ✓ | - | - | 20.9% |
| M | ✓ | - | ✓ | - | 71.5% |
| G | ✓ | - | - | ✓ | 1.1% |
| TM | ✓ | ✓ | ✓ | - | 95.2% |
| TG | ✓ | ✓ | - | ✓ | 21.6% |
| MG | ✓ | - | ✓ | ✓ | 88.4% |
| TMG | ✓ | ✓ | ✓ | ✓ | 100% |

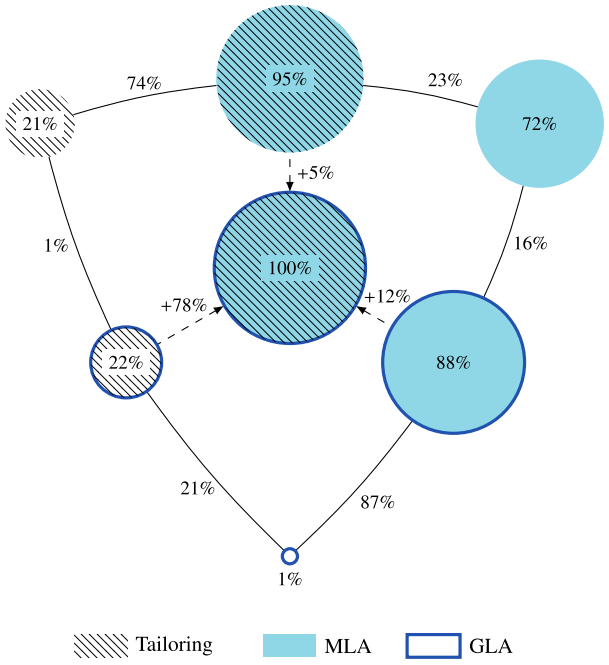


**Fig. 7.** Normalised mass reduction obtained in the optimisations and the differences between the various combinations. The area of the circles corresponds to the normalised mass reduction. 100% signifies the maximum achievable mass reduction combining structural tailoring, MLA and GLA.

(N) is an optimization where neither active control, i.e. MLA and GLA, nor passive structural adaptation is considered. Besides optimisations including the different methods alone (T, M, G), their possible combinations are considered (TM, TG, MG, TMG). In the following, the achieved mass reduction relative to the reference case is normalised to the reduction obtained by the optimisation in which all design variables are active (TMG). The achieved normalised mass reduction in each of the optimisations is also given in Table 2. As expected, the maximum achievable reduction in primary wing structural mass is obtained by the TMG optimisation. It can be seen that the sum of the results of the optimisations with the individual methods is smaller than the results of the combined methods. For example, the sum of the results of the T, M and G optimisation yields a normalised mass reduction of 94% being six per cent lower than the result in the concurrent optimisation (TMG, 100%). This indicates that the various methods interact in a synergistic way that, of course, is only revealed in simultaneous optimisations.

The results are illustrated in Fig. 7 in which the area of each circle corresponds to the obtained normalised mass reduction. Also, the differences between the optimisation results are shown. The most synergistic effect is observed in the combination of active

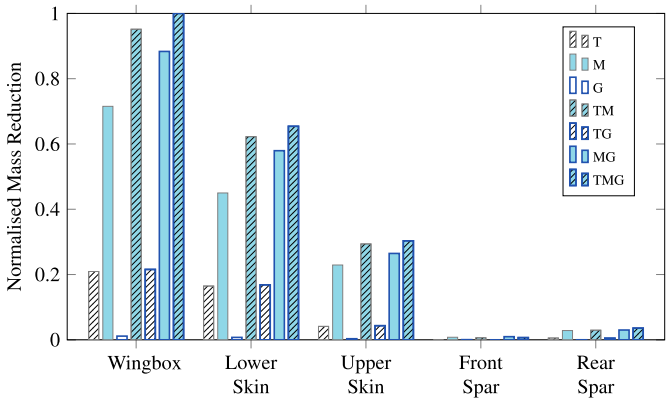


**Fig. 8.** Componentwise mass reduction obtained in the optimisations normalised to the achievable mass reduction obtained in the TMG optimisation.

manoeuvre and gust load alleviation. While the sum of normalised mass reduction achieved by the separate use of the active control methods results in 73% (M+G), the combined use yields a 15% higher mass reduction of 88% of the maximum achievable mass reduction. This significant synergistic effect between MLA and GLA has been observed before [19]. A similar though less remarkable trend is visible in the combination of MLA with structural tailoring resulting in a two per cent higher mass saving than the sum of the savings obtained in the optimisations with the individual technologies. In contrast, no synergistic effect is observed by the combination of GLA and structural tailoring. Here the sum of the effects obtained in separate optimisations equals the effect observed in the optimisation with the combined use. It is furthermore worth noting that, the mass reduction obtained by MLA is underestimated when optimised individually compared to a combination with GLA, structural tailoring or both. The same is observed for GLA where the effect in the individual optimisation is only a normalised mass reduction of one per cent compared to for example an added value of 16% (MG-M) in the combined use with MLA or only five per cent (TMG-TM) in the combined use with MLA and structural tailoring. For structural tailoring, this does not hold. The added value of tailoring is 12% when combined with active control (TMG-MG) being nine per cent lower than observed in the individual optimisation (T: 21%).

To understand the interaction, the normalised mass reduction in the individual wingbox components given in Fig. 8 shows, that the main focus needs to be placed on the driving constraints in the skins. Although optimising the spars does not contribute to the overall mass reduction, their consideration in the optimisation problem is still important because of their contribution to the overall stiffness distribution of the wingbox. The ratio between manoeuvre and gust constraints in the skins over the spanwise position is shown in Fig. 9. Values of more than one indicate areas where manoeuvres are critical, less than one where gusts dimension the wing. While the wing resulting from the N optimisation is both, dimensioned by manoeuvres and gusts, the application of MLA in the M optimisation makes most of the wing structure gust-critical. In contrast to that, the application of GLA in the G optimisation results in a entirely manoeuvre driven design. The values at the tip are irrelevant, as the thickness reaches the minimum allowable thickness, resulting in a locally oversized structure where neither gust nor manoeuvre constraints are active.

These results explain the synergy between MLA and GLA that can be observed in MG optimisation, as each of the two methods allows more opportunities for the other. The application of structural tailoring in the T optimisation is less influential to the constraint ratio than the active control methods but increases the manoeuvre criticality slightly compared to the reference N. This increase in manoeuvre criticality due to structural tailoring explains (i) that the application of GLA (TG vs T) can not result in more benefits than observed in the individual optimisation (G vs N), and (ii) the synergistic effect in the combination of MLA and structural tailoring.

For further analysis of the mechanism of structural tailoring in the presence of active control, the nondimensional bending-torsion coupling ratio as defined by [4] is used:

$$\Psi = \frac{K}{\sqrt{EI\,GJ}} \tag{6}$$

with $EI$ being the bending stiffness, $GJ$ the torsional stiffness and $K$ the bending-torsion coupling stiffness. Positive values of $\Psi$ indicate a positive bending-torsion coupling, also known as wash-in, i.e. upward bending accompanied by a nose up twist. Negative values relate to the desired wash-out, i.e. upward bending accompanied by a nose-down twist shifting the centre of load inboard.

The characteristics of the distribution of tailoring induced bending-torsion coupling shown in Fig. 10 are similar with and without MLA (T vs TM), except for the tip, that is less important for the overall load redistribution. Especially notable is that in the presence of MLA, the optimiser increases the amount of wash-out even though the negative bending-torsion coupling has a negative effect on the control surface effectiveness as shown by Weisshaar [4].

With the addition of GLA, the optimiser reduces the amount of negative bending-torsion coupling in the outboard area of the wing. In the TG optimisation, only the very outboard part is affected but comparing TMG and TM, the addition of GLA significantly influences the characteristics of the bending-torsion coupling distribution.

As the design resulting from the TM optimisation is mainly gust-critical, the application of GLA requires the optimiser to increase the effectiveness of GLA by strengthening the authority the control surfaces have in controlling the gust loads. To support this thesis, we define the $\mathcal{H}_2$ norm of the transfer function of a control surface input to a bending load output as a measure for the load control authority. The $\mathcal{H}_2$ norm is computed with and without structural tailoring, i.e. $\phi_{\text{lo}}, \phi_{\text{up}}$ are set to zero after the optimisation, to characterise the influence of structural tailoring on the load control authority. The relative difference is given by:

$$\Delta_{\mathcal{H}_2} = \frac{\mathcal{H}_2}{\mathcal{H}_{2,\phi=0}} - 1 \tag{7}$$

The relative difference in the $\mathcal{H}_2$ norm of transfer functions from the ailerons to various spanwise load outputs is shown in Fig. 11. In all cases, structural tailoring reduces the bending load control authority of both ailerons with the outer aileron being more affected. As initially expected, the structural tailoring in the TMG optimisation has less detrimental effect on the load control authority compared to the TM optimisation.

In addition to the described differences in structural tailoring, the differences in MLA design are discussed next. As an example, the control surface deflections given by the optimised MLA during the push-over manoeuvre are shown in Fig. 12. In all optimisations except for the M optimisation, the -1 g manoeuvre contributes to the critical loads, and the optimiser uses MLA to redistribute the loads, reducing the level of constraints. Except for the outer aileron, which in all cases is deflected downwards to unload the wing tip, the characteristics of the MLA deflections are different between the cases with (TM and TMG) and without (MG) structural tailoring. Without tailoring, the deflections increase towards the tip while with tailoring, the deflections are reduced towards the tip. The latter is the expected pattern shifting the load inboard and is similar to the patterns found by Stanford [43] and Krupa et

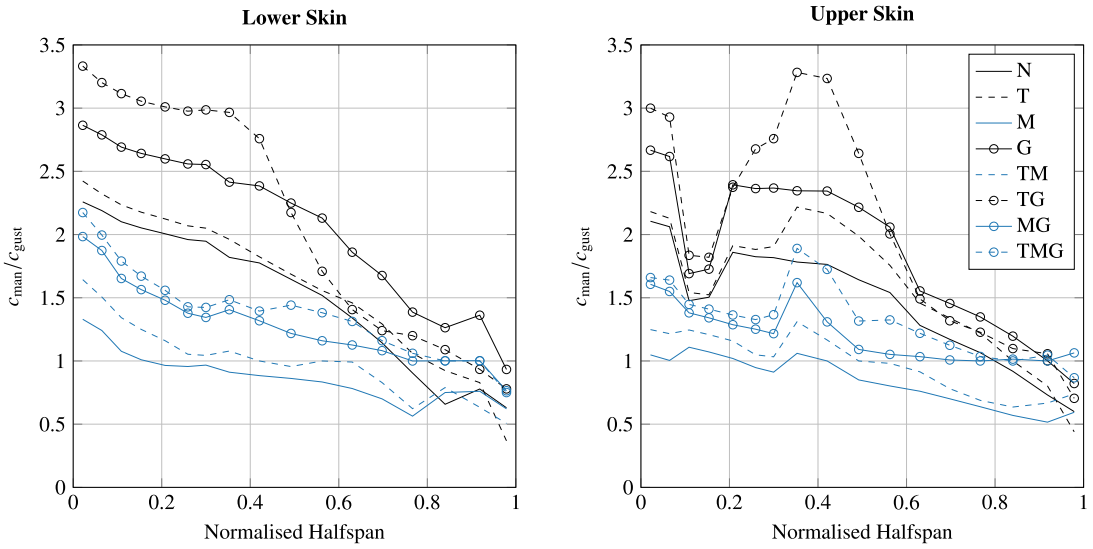


**Fig. 9.** Spanwise distribution of the ratio between manoeuvre and gust constraints.

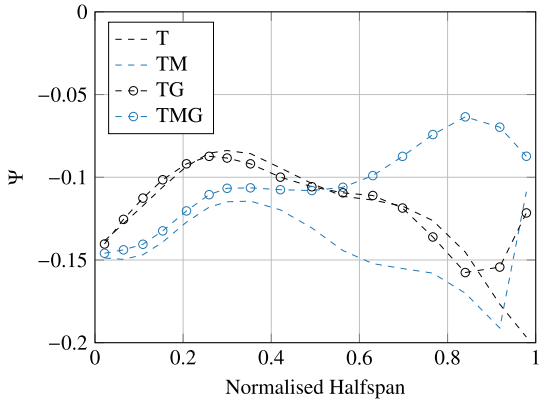


**Fig. 10.** Spanwise distribution of the bending-torsion coupling parameter Ψ.

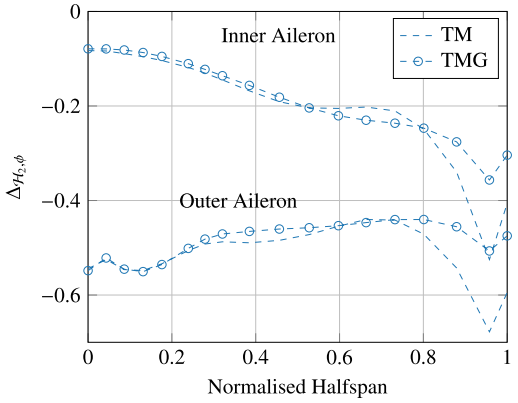


**Fig. 11.** Effect of structural tailoring on spanwise load control authority characterized by the relative difference in the $\mathcal{H}_2$ norm of the transfer function from a control surface input to a spanwise bending load output with and without structural tailoring.

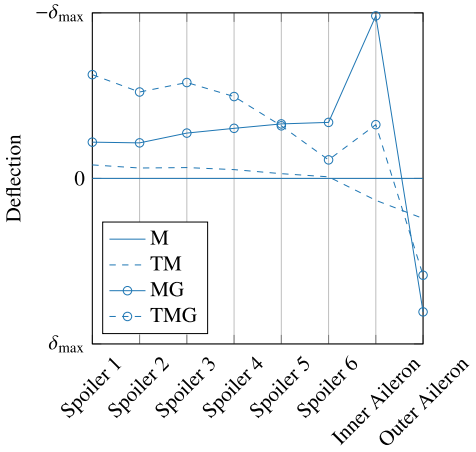


**Fig. 12.** Optimised control surface deflections for MLA during the push-over manoeuvre.

**Table 3**
Relative difference in the first symmetric bending frequency of the resulting wing structures obtained in the different optimisations compared to N.

| Optimisation | First Sym. Bending Frequency Difference |
|---|---|
| T | -9.2% |
| M | -12.4% |
| G | -0.1% |
| TM | -25.2% |
| TG | -9.4% |
| MG | -15.8% |
| TMG | -25.9% |

al. [27]. While finding the exact reason for the pattern observed in the MG optimisation would require further analysis, the different characteristics justify the need for an integrated design of MLA together with the variables of the structural tailoring to make optimal use of both technologies.

Due to the dynamic nature of gust encounters, the design differences in the GLA system are even more challenging to grasp. However, the primary influence on the control law can be linked to the first symmetric bending mode frequency that, for the given type of configuration, governs the dynamic gust loads [44].

The frequency response of the FIR filter associated with the fifth spoiler, including the high-pass filter of the AOA probe is shown in Fig. 13. The frequency response characteristics of the filter, e.g. the peak position, resulting from the various optimisations are different due to the variation of the structural eigenfrequencies given in 3.

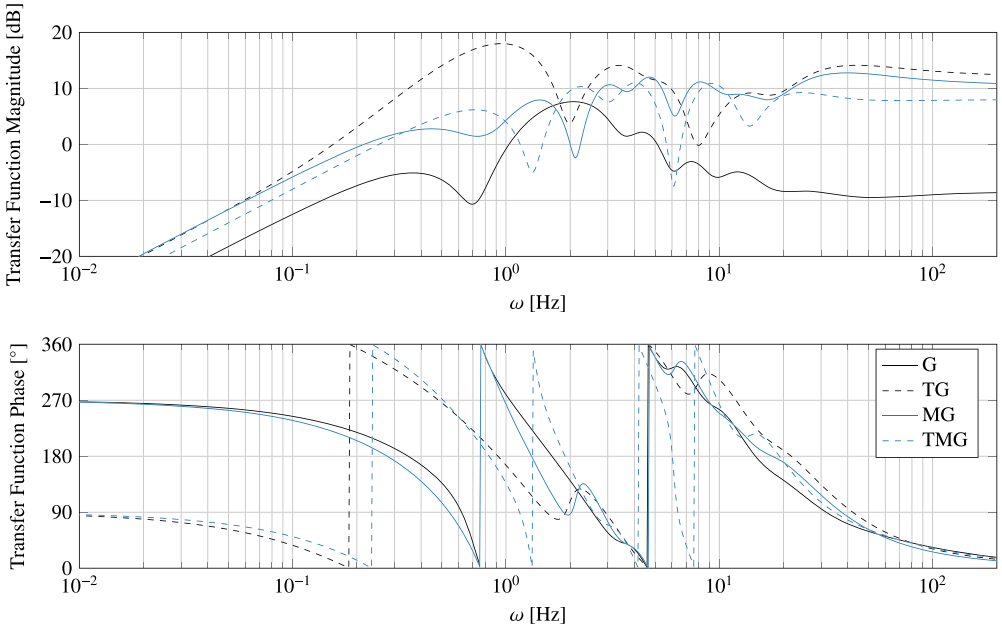


**Fig. 13.** Bode plot of the frequency response of the optimal FIR filter associated to the fifth spoiler as optimised in the different setups including GLA.

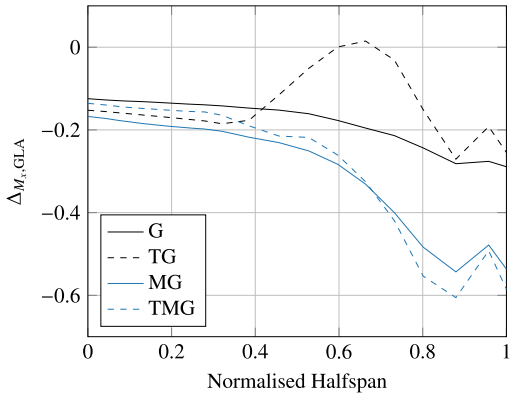


**Fig. 14.** Relative difference between the open and closed loop spanwise maximum bending moment distribution during gust encounters.

The difference in the resulting GLA mechanism is analysed by a comparison of the relative difference on the maximum bending moment around the longitudinal axis $x$ between open loop and closed loop gust loads defined as:

$$\Delta_{M_x,\mathrm{GLA}} = \frac{\max(M_{x,\mathrm{gust,open\ loop}})}{\max(M_{x,\mathrm{gust,closed\ loop}})} - 1 \tag{8}$$

The relative difference in the maximum bending moment distribution is shown in Fig. 14 for the different controllers resulting from the optimisations G, TG, MG and TMG. A significant difference is visible between the cases with and without manoeuvre load alleviation (G and TG vs MG and TMG). Due to the reduced stiffness, the controller is much more effective in reducing the gust loads. Another interesting point is that in the TG optimisation, the optimiser even allows the controller to increase the bending loads at a mid-wing position of 60-70% of the normalised halfspan, as this region is not dimensioned by gust loads, see Fig. 9. This means the optimiser adopts the mechanism to the prevailing load hierarchy.

In conclusion, only the simultaneous design of GLA with MLA and structural tailoring can exploit the full potential.

### 4.3. Sensitivity of material properties knockdown factor

In the design of safety-critical aircraft structures, the nominal allowables are significantly reduced by knockdown factors accounting for low-speed impact damage, material scatters and environmental effects as temperature, moist and UV light [45]. A variety of knockdown factors is investigated because new design paradigms and materials are envisioned in the future. The inclusion of fatigue models in the optimisation problem could replace the respective knockdown factors allowing for more flexible wing designs [46]. Also, the development of materials with significantly higher allowables, e.g. carbon nanotubes, can reduce the stiffness of future wing structures drastically [47].

While most of the examples listed in the introduction give no information on the applied knockdown factor, there are also studies which do not consider any knockdown factor [48], [49]. Other studies use maximum strain allowables that are more conservative [27].

The results shown in the previous section were produced with a knockdown factor of 0.65 applied to the material strength properties, i.e. longitudinal/transverse tension/compression strength as well as the in-plane shear strength. In this section, the knockdown factor is gradually changed from 0.35 to 0.95 to investigate the effect of the material properties on the main findings of the previous section.

Fig. 15 shows the resulting primary structural mass for various knockdown factors normalised to the primary structural mass obtained in the N optimisation using a knockdown factor of 0.65. A reduction of the knockdown factor from 0.65 to 0.35 results in an increase of the optimised mass of 100% in the absence of active control and structural tailoring (N). The sensitivity is less pronounced when all technologies are present (TMG). It is worth noting that, an increase in the material knockdown factor of 0.01 corresponds to a mass reduction of 1.60% in the N optimisations compared to 0.75% in the TMG optimisations. The net benefit of new material technologies should therefore always be assessed with taking into account all system and technologies that influence the loads on the wing structure.

The influence of the material knockdown factor on the mass reduction achievable by the individual technologies and their combinations is given in Fig. 16. The mass reduction achievable by

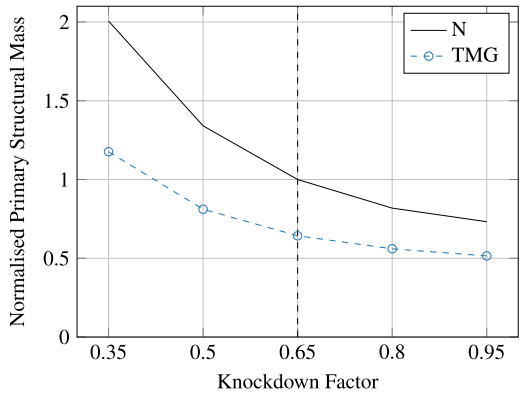


**Fig. 15.** Influence of the material knockdown factor on resulting objective function, namely primary structural mass, normalised to the objective resulting from the N optimisation with a knockdown factor of 0.65.

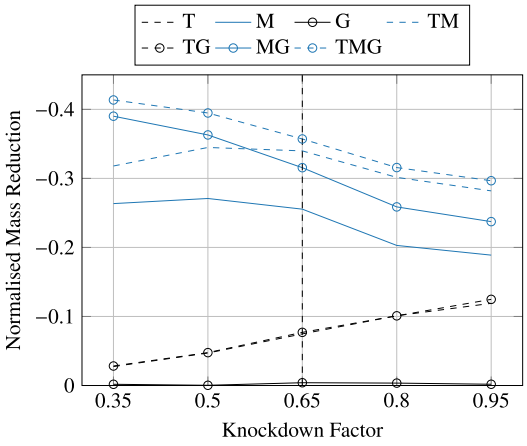


**Fig. 16.** Influence of the material knockdown factor on the mass reduction normalised with respect to the N optimisations.

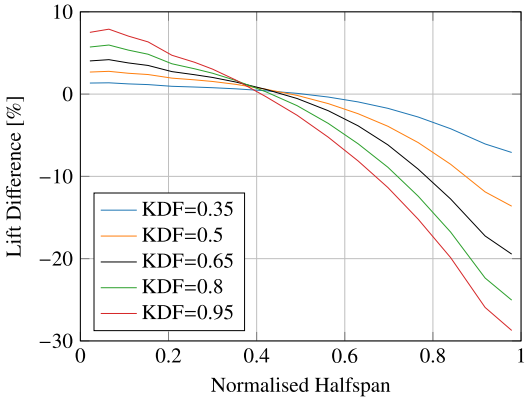


**Fig. 17.** The difference in the lift distribution during the 2.5 g manoeuvre due to structural tailoring (T vs N) for different knockdown factors.

structural tailoring is increasing with higher knockdown factors, i.e. more flexible and hence less stiff structures. The effect of the knockdown factor on the tailoring-induced difference in the pull-up manoeuvre lift distribution (T vs N) is given in Fig. 17. With higher knockdown factors and less bending stiffness, the bending-torsion coupling induced by structural tailoring is resulting in more wash-out by higher deflecitons.

The potential of MLA is, as expected, negatively affected by higher knockdown factors as the higher flexibility has detrimental effects on the control surface effectiveness.

For the investigated range of knockdown factors, the individual application of GLA is not leading to any mass reduction as for all N optimisations the gust constraints are below the manoeuvre constraint level.

For all used knockdown factors, tailoring is increasing the manoeuvre criticality which explains that no interaction with GLA is observed in the absence of MLA. It is interesting to note that for all knock factors, GLA only has added value if MLA is active. The interplay of MLA and GLA observed in the MG and TMG optimisations is improved for lower knockdown factors, which can be linked to the higher control surface effectiveness that comes with stiffer wings.

In total, a substantial shift of effectiveness from active GLA to passive structural tailoring is observed with increasing structural flexibility. For a knockdown factor of 0.35, the combination of MLA and GLA can lead to 94% of the possible mass reduction reducing the added value of structural tailoring to six per cent. For knockdown factors higher than 0.65, the added value of active GLA shrinks down to less than five per cent of the achievable mass reduction. That means that with the trend of increasing material allowables and the industrialisation of structural tailoring, the mass saving potential of GLA is reduced. However, the added value of MLA is still significant.

## 5. Conclusions

The interaction between the three technologies of active manoeuvre load alleviation, gust load alleviation and structural tailoring has been investigated. The simultaneous design optimisation of a wing structure together with the control system was carried out on the example of a typical long-haul transport aircraft configuration. The optimisations with the individual technologies and their combinations reveal, that, as already found by previous research, the maximum reduction in primary wing structural mass is achieved by a concurrent use of all three technologies. The discussed design differences that are observed in the individual and combined optimisations indicate that combined optimisation is required to (i) exploit the synergies of active control and structural tailoring to the full extent and (ii) to assess the potential of each of the technologies correctly.

An investigation of the sensitivity of the results regarding the knockdown factor applied to the material properties showed that with increasing structural flexibility a significant shift in effectiveness from active gust load control to passive structural tailoring is observed. While the increasing material allowables and the exploitation of the anisotropic material properties promise significant mass savings, the relative potential of the active gust load control is reduced. The net benefit of new material technologies should, therefore, be assessed by taking into account active control.

As the present work involves a generally idealised approach for active load alleviation and structural tailoring, future studies would benefit from more refined implementations. These enhancements could include stacking sequence optimisation, manufacturing constraints, chordwise thickness variation or stringer shape and geometry optimisation as well as failure scenarios and more detailed constraints, e.g. including continuous turbulence load conditions. Especially the consideration of low speed handling qualities is essential as they are defining the required control surface effectiveness of the outboard aileron. The aerodynamic modelling approach would benefit from the consideration of compressible and transonic effects enabling the inclusion of stability constraints that are important for high aspect ratio wing designs. With the introduction of flutter constraints, flutter suppression methods need to be considered alongside. Further studies are also required tp assess the transferability of the main results of this work to other aircraft configurations and sizes.

## Declaration of competing interest

The authors declare that they have no known competing financial interests or personal relationships that could have appeared to influence the work reported in this paper.

## Acknowledgements

The authors want to thank Paul Lancelot from Delft University of Technology for providing the CFD data used for the derivation of the correction law of the downwash distribution used for modelling spoiler deflections with panel based aerodynamic models.

This research did not receive any specific grant from funding agencies in the public, commercial, or not-for-profit sectors.

## References

[1] H. Rösner, K. Jockel-Miranda, Airbus airframe – new technologies and management aspects, Materialwissenschaft und Werkstofftechnik 37 (9) (2006) 768–772, https://doi.org/10.1002/mawe.200600062.
[2] M.M. Munk, Laminated propeller, U.S. patent no. 2,599,718, 1949.
[3] M.H. Shirk, T.J. Hertz, T.A. Weisshaar, Aeroelastic tailoring - theory, practice, and promise, J. Aircr. 23 (1) (1986) 6–18, https://doi.org/10.2514/3.45260.
[4] T.A. Weisshaar, Aeroelastic tailoring - creative uses of unusual materials, in: AIAA/ASME/ASCE AHS 28th Structures, Structural Dynamics and Materials Conference, 1987.
[5] T.-U. Kim, I.H. Hwang, Optimal design of composite wing subjected to gust loads, Comput. Struct. 83 (19-20) (2005) 1546–1554, https://doi.org/10.1016/j.compstruc.2005.02.002.
[6] G.K.W. Kenway, J.R.R.A. Martins, Multipoint high-fidelity aerostructural optimization of a transport aircraft configuration, J. Aircr. 51 (1) (2014) 144–160, https://doi.org/10.2514/1.C032150.
[7] J.K.S. Dillinger, M.M. Abdalla, T. Klimmek, Z. Gürdal, Static aeroelastic stiffness optimization and investigation of forward swept composite wings, in: World Congress on Structural and Multidisciplinary Optimization, 2013.
[8] G.J. Kennedy, J.R.R.A. Martins, A comparison of metallic and composite aircraft wings using aerostructural design optimization, in: AIAA Aviation Technology, Integration, and Operations (ATIO) Conference and 14th AIAA/ISSM, 2012.
[9] T. Farsadi, D. Asadi, H. Kurtaran, Flutter improvement of a thin walled wing-engine system by applying curvilinear fiber path, Aerosp. Sci. Technol. 93 (2019) 105353, https://doi.org/10.1016/j.ast.2019.105353.
[10] A. Viglietti, E. Zappino, E. Carrera, Free vibration analysis of variable angle-tow composite wing structures, Aerosp. Sci. Technol. 92 (2019) 114–125, https://doi.org/10.1016/j.ast.2019.05.068.
[11] O. Stodieck, J.E. Cooper, P.M. Weaver, P. Kealy, Aeroelastic tailoring of a representative wing box using tow-steered composites, AIAA J. 55 (4) (2017) 1425–1439, https://doi.org/10.2514/1.J055364.
[12] C.D. Regan, C.V. Jutte, Survey of applications of active control technology for gust alleviation and new challenges for lighter-weight aircraft: Nasa/tm-2012-216008.
[13] T.A. Weisshaar, Aeroelastic tailoring of forward swept composite wings, J. Aircr. 18 (8) (1981) 669–676, https://doi.org/10.2514/3.57542.
[14] E. Livne, Integrated aeroservoelastic optimization: status and direction, J. Aircr. 36 (1) (1999) 122–145, https://doi.org/10.2514/2.2419.
[15] T.A. Zeiler, T.A. Weisshaar, Integrated aeroservoelastic tailoring of lifting surfaces, J. Aircr. 25 (1) (1988) 76–83, https://doi.org/10.2514/3.45544.
[16] L. Librescu, L. Meirovitch, O. Song, Integrated structural tailoring and control using adaptive materials for advanced aircraft wings, J. Aircr. 33 (1) (1996) 203–213, https://doi.org/10.2514/3.46923.
[17] T.A. Weisshaar, D.K. Duke, Induced drag reduction using aeroelastic tailoring with adaptive control surfaces, J. Aircr. 43 (1) (2006) 157–164, https://doi.org/10.2514/1.12040.
[18] T.A. Weisshaar, D.K. Duke, A. Dobbins, Active aeroelastic tailoring with adaptive continuous control surfaces, in: AIAA Structures, Structural Dynamics, and Materials Conference and Exhibit, 2000.
[19] J. Xu, I. Kroo, Aircraft design with active load alleviation and natural laminar flow, J. Aircr. 51 (5) (2014) 1532–1545, https://doi.org/10.2514/1.C032402.
[20] B.K. Stanford, C.D. Wieseman, C.V. Jutte, Aeroelastic tailoring of transport wings including transonic flutter constraints, in: AIAA/ASCE/AHS/ASC Structures, Structural Dynamics, and Materials Conference, 2015.
[21] B.K. Stanford, Optimization of an aeroservoelastic wing with distributed multiple control surfaces, J. Aircr. 53 (4) (2016) 1131–1144, https://doi.org/10.2514/1.C033613.
[22] B.K. Stanford, Static and dynamic aeroelastic tailoring with variable-camber control, J. Guid. Control Dyn. 39 (11) (2016) 2522–2534, https://doi.org/10.2514/1.G000413.
[23] B.K. Stanford, Aeroservoelastic optimization under stochastic gust constraints, in: AIAA Applied Aerodynamics Conference, 2018.
[24] D.A. Burdette, J.R.R.A. Martins, Design of a transonic wing with an adaptive morphing trailing edge via aerostructural optimization, Aerosp. Sci. Technol. 81 (2018) 192–203, https://doi.org/10.1016/j.ast.2018.08.004.
[25] V.H. Handojo, P. Lancelot, R. De Breuker, Implementation of active and passive load alleviation methods on a generic mid-range aircraft configuration, in: AIAA Multidisciplinary Analysis and Optimization, 2018.
[26] N.P.M. Werter, Aeroelastic Modelling and Design of Aeroelastically Tailored and Morphing Wings, PhD Thesis, 2017.
[27] E.P. Krupa, J.E. Cooper, A. Pirrera, R. Nangia, Improved aerostructural performance via aeroservoelastic tailoring of a composite wing, Aeronaut. J. 122 (1255) (2018) 1442–1474, https://doi.org/10.1017/aer.2018.66.
[28] K. Seywald, Impact of Aeroelasticity on Flight Dynamics and Handling Qualities of Novel Aircraft Configurations, PhD Thesis, ISBN 978-3-8439-3076-5, 2016.
[29] E.A. Ferede, M.M. Abdalla, Cross-sectional modelling of thin-walled composite beams, in: AIAA/ASME/ASCE/AHS/ASC Structures, Structural Dynamics, and Materials Conference, 2014.
[30] N.P.M. Werter, R. De Breuker, A novel dynamic aeroelastic framework for aeroelastic tailoring and structural optimisation, Compos. Struct. 158 (2016) 369–386, https://doi.org/10.1016/j.compstruct.2016.09.044.
[31] S.G. Hedman, Vortex lattice method for calculation of quasi steady state loadsings on thin elastic wings in subsonic flow, FFA Report 105, The Aeronautical Research Institute of Sweden, 1966.
[32] M. Mohammadi-Amin, B. Ghadiri, M.M. Abdalla, H. Haddadpour, R. De Breuker, Continuous-time state-space unsteady aerodynamic modeling based on boundary element method, Eng. Anal. Bound. Elem. 36 (5) (2012) 789–798, https://doi.org/10.1016/j.enganabound.2011.12.007.
[33] N.P.M. Werter, R. De Breuker, M.M. Abdalla, Continuous-time state-space unsteady aerodynamic modeling for efficient loads analysis, in: International Forum on Aeroelasticity and Structural Dynamics, 2015.
[34] S. Binder, A. Wildschek, R. De Breuker, Extension of the continuous time unsteady vortex lattice method for arbitrary motion, control surface deflection and induced drag calculation, in: International Forum on Aeroelasticity and Structural Dynamics, 2017.
[35] J. Vassberg, M. Dehaan, M. Rivers, R. Wahls, Development of a common research model for applied cfd validation studies, in: 26th AIAA Applied Aerodynamics Conference, American Institute of Aeronautics and Astronautics, Reston, VA, 2008, p. 2001.
[36] S. Binder, A. Wildschek, R. De Breuker, Unsteady aerodynamic model order reduction for aeroservoelastic optimisation by balanced proper orthogonal decomposition and the use of synthetic mode shapes, J. Aeroelasticity Struct. Dyn. 6 (1) (2018) 43–72, https://doi.org/10.3293/asdj.2018.49.
[37] S. Binder, A. Wildschek, R. De Breuker, Aeroelastic stability analysis of the flexop demonstrator using the continuous time unsteady vortex lattice method, in: AIAA/ASCE/AHS/ASC Structures, Structural Dynamics, and Materials Conference, 2018.
[38] S.J. Elliot, Signal Processing for Active Control, Elsevier, 2001.
[39] S.T. IJsselmuiden, M.M. Abdalla, Z. Gürdal, Implementation of strength-based failure criteria in the lamination parameter design space, AIAA J. 46 (7) (2008) 1826–1834, https://doi.org/10.2514/1.35565.
[40] J.K.S. Dillinger, T. Klimmek, M.M. Abdalla, Z. Gürdal, Stiffness optimization of composite wings with aeroelastic constraints, J. Aircr. 50 (4) (2013) 1159–1168, https://doi.org/10.2514/1.C032084.
[41] G. Kreisselmeier, R. Steinhauser, Systematic control design by optimizing a vector performance index, Comput. Aided Des. Control Syst. (1980) 113–117, https://doi.org/10.1016/B978-0-08-024488-4.50022-X.
[42] European Union Aviation Safety Agency, Certification specifications and acceptable means of compliance for large aeroplanes (cs-25), Amendment 23 (2019).
[43] B.K. Stanford, Optimal control surface layout for an aeroservoelastic wingbox, AIAA J. 55 (12) (2017) 4347–4356, https://doi.org/10.2514/1.J056070.
[44] A. Wildschek, An Adaptive Feed-Forward Controller for Active Wing Bending Vibration Alleviation on Large Transport Aircraft, PhD Thesis, 2008.
[45] C. Kassapoglou, Design and Analysis of Composite Structures: With Applications to Aerospace Structures, John Wiley & Sons, 2013.
[46] D. Rajpal, C. Kassapoglou, R. De Breuker, Aeroelastic optimization of composite wings subjected to fatigue loads, in: AIAA/ASCE/AHS/ASC Structures, Structural Dynamics, and Materials Conference, 2018.
[47] G.J. Kennedy, G.K.W. Kenway, J.R.R.A. Martins, High aspect ratio wing design: optimal aerostructural tradeoffs for the next generation of materials, in: AIAA Aerospace Sciences Meeting, 2014.
[48] T.R. Brooks, J.R.R.A. Martins, High-fidelity multipoint aerostructural optimization of a high aspect ratio tow-steered composite wing, in: AIAA/ASCE/AHS/ASC Structures, Structural Dynamics, and Materials Conference, 2017.
[49] K.R.B. Bramsiepe, V.H. Handojo, Y.M. Meddaikar, M. Schulze, T. Klimmek, Loads and structural optimisation process for composite long range transport aircraft configuration, in: AIAA Multidisciplinary Analysis and Optimization, 2018.